No. 68-129

EXPERIMENTS IN SUPERSONIC TURBULENT FLOW WITH LARGE DISTRIBUTED SURFACE INJECTION

by

F. L. FERNANDEZ and E. E. ZUKOSKI
California Institute of Technology
Pasadena, California

AIAA Paper
No. 68-129

AIAA 6th Aerospace Sciences Meeting

NEW YORK, NEW YORK/JANUARY 22-24, 1968

EXPERIMENTS IN SUPERSONIC TURBULENT FLOW WITH LARGE DISTRIBUTED SURFACE INJECTION†

F. L. Fernandez* and E. E. Zukoski**
California Institute of Technology
Pasadena, California

Abstract

The mean velocity and pressure fields in a turbulent boundary layer on a flat plate at $M_\infty = 2.6$ are investigated for ratios of mass flow per unit area injected at the wall to that at the edge of the boundary layer (λ_e) between 0 and 0.03. Two-dimensionality is demonstrated, and a similar flow established with linear growth of momentum and displacement thicknesses. A Howarth-Dorodnitsyn transformation for the normal coordinate is found to bring the data into good agreement with incompressible results for the same value of λ_e. At the highest injection rate, the velocity profiles agree well with turbulent mixing-layer results. However, unlike mixing layers, the maximum rate of mass entrainment is the same as for the incompressible case. Finally, the induced side forces are found to be comparable to those obtained by equivalent injection through a slot.

Symbols

C_f	skin friction coefficient, $2\tau_w/\rho_e u_e^2$
F	side force
H	form parameter, δ^*/θ
H_i	incompressible form parameter, $\overline{\delta^*}/\overline{\theta}$
M	Mach number
$Re\theta$	Reynolds number, based on edge conditions, $(\rho_e u_e \theta)/\mu_e$
T	temperature
T_t	total temperature
u	velocity component in x-direction
v	velocity component in y-direction
x	distance along plate measured from start of porous region
y	distance normal to wall
$\overline{y}/\overline{\theta}$	transformed distance normal to wall, $\overline{y}/\overline{\theta} = \int_0^y \frac{\rho}{\rho_e} d(y/\theta)$
δ^*	displacement thickness, $\int_0^\delta (1-\rho u/\rho_e u_e)dy$
δ	edge of layer
θ	momentum thickness, $\int_0^\delta \rho u/\rho_e u_e(1-u/u_e)dy$
$\overline{\delta^*}$	incompressible displacement thickness, $\int_0^{\overline{\delta}} (1-\overline{u}/\overline{u}_e)d\overline{y}$
Θ	induced flow angle at edge $= v_e/u_e$
$\overline{\theta}$	incompressible momentum thickness, $\int_0^{\overline{\delta}} \overline{u}/\overline{u}_e(1-\overline{u}/\overline{u}_e)d\overline{y}$
λ_e	$\rho_w v_w/\rho_e u_e$
λ_∞	$\rho_w v_w/\rho_\infty u_\infty$
μ	viscosity
η, ξ, σ	transformation functions
ψ	stream function; $\partial\psi/\partial y = \rho u$, $\partial\psi/\partial x = -\rho v$
τ	shear stress
ρ	density

Subscripts

w	wall value
e	value at edge of layer
∞	free stream value

bars above quantities denote values for an incompressible flow ($\overline{\rho}$ = const).

I. Introduction

The normal injection of gas through a porous wall into a two-dimensional, turbulent boundary layer bounded by a supersonic stream can produce large changes in flow inclination angles and can induce an appreciable increase in surface pressure. At least three regimes exist for the uniform blowing problem in a supersonic flow. First, when the skin friction term in the integrated momentum equation is comparable to or larger than the injectant term, both skin friction and injectant flow rate influence the problem. Although the boundary layer theory is applicable, no simple, self-similar solution can be obtained because of the skin friction term. Second, when the injectant term is very large compared with the skin friction term but the injectant momentum flux is small compared with the free-stream momentum flux, the boundary layer approach is still valid, and now self-similar solutions with a uniform external flow become possible. Finally, when the momentum flux of the injectant and free stream are comparable, the boundary layer approach is not applicable. The problem studied in this paper is the second one, and the terms 'large blowing rate' or 'strong blowing' will be used to describe this (second) regime, in contrast to the first one. The conditions obtained in this study never approach those of the third regime. A schematic diagram for the flow field and pressure distribution for the second case is shown in Figure 1.

A survey of the literature indicates that both for low speed and compressible flow, the effect of injection has been experimentally investigated, primarily with the view of determining the effects on skin friction and heat transfer. Because of this, the data quoted in the literature are for injection rates so low that the velocity profiles, though altered, can still be regarded as slightly perturbed boundary-layer profiles.

---

† This work was supported by the U. S. Army Research Office and the Advanced Research Projects Agency, Contract No. DA-31-124-ARO(D)-33.

* Graduate Student, Department of Aeronautics.

** Professor of Engineering and Jet Propulsion, Daniel and Florence Guggenheim Jet Prop. Center.

Recent experiments have been performed by Hartunian and Spencer[1] at $M_\infty = 4.5$ for flow that was probably laminar and for truly massive injection rates. Unfortunately, the nature of their experiment did not allow for careful probing of the layer to determine velocity profiles.

Incompressible data on turbulent flows with large injection have been reported by McQuaid[2] and Mugalev[3]. Mugalev's experiments were conducted on a plate mounted in a free jet. Because velocity profiles are given for only two stations in the flow, and no attempt was made to monitor or control the static pressure, these data are suspect. In a more carefully controlled experiment, McQuaid used a flexible tunnel wall to maintain the tunnel static pressure constant and made detailed velocity measurements for a wide range of injection rates. Experimental data on compressible turbulent flows with large injection seem virtually nonexistent.

This paper discusses an experiment in which a similar, two-dimensional turbulent flow is established by large blowing into a turbulent boundary layer. The mean flow quantities are measured and analyzed to determine the effect of the blowing rate and compressibility.

II. Experimental Procedure

The experiments were conducted in the Supersonic Wind Tunnel of the Graduate Aeronautical Laboratories, California Institute of Technology (GALCIT). The tunnel test section is 2 inches by $2\frac{1}{2}$ inches and the tunnel operates at a Mach number of 2.6. The stagnation conditions for all runs were a pressure of 740 mm Hg and a temperature of 80° F. The boundary layer on the tunnel wall was tripped near the nozzle throat to ensure turbulent flow in the test section. At the start of injection, the boundary layer is about 0.12 inches thick. The model consists of a uniformly porous, stainless-steel insert, 3.4 inches long by 2 inches wide, which forms part of the test section wall and is separated from the tunnel side walls by swept fences. Figure 2 is a schematic of the model mounted in the tunnel. Air was used as the injectant in the experiments. The total mass flow of air through the plate was measured, along with the temperature of the air in the model plenum and the back-face temperature of the porous plate. Both of these temperatures were found to be within a few degrees of the tunnel stagnation temperature for all runs. The ratio of wall mass flow per unit area to that in the free stream was varied from 0 to 0.045.

During the experiments, schlieren photographs were taken to determine the induced shock angles. Centerline pitot-tube measurements were made using a flattened boundary-layer probe at a series of stations in the flow for each of the injection rates considered. The pitot tube used in the experiments was fabricated from .083 inch o. d. stainless-steel tubing with a tip flattened to .007 inches by .100 inches and an opening of about .004 inches. Thus, readings to within .004 inches from the wall were possible. The pitot was pitched down at an angle of about 10° to the horizontal to allow minimum angle of attack effect within the injection layer. Experiments showed that the probes used in these tests were insensitive to angle of attack variations of $\pm 10^\circ$ for subsonic and supersonic flows.

The pitot pressure and y-position data were recorded using a Statham pressure transducer and a 40-turn helipot whose outputs were connected directly to an x-y plotter. The horizontal and vertical pitot drives used were accurate to within .001 inches. Pitot tube contact with the wall was determined electrically. Very near the surface of the plate, where the streamlines are strongly curved, the pitot readings will have large errors due to the large angle of attack of the flow relative to the pitot axis. It was decided to take the pitot data first and then to decide the effect of this error on the overall measurements. Static pressures were directly measured ahead of and behind the model (centerline and spanwise) and on the fences. Pressure tap locations are shown schematically in Figure 2.

Porous Plate Calibration

The first stage of the experiment was devoted to determining the spatial uniformity of the porous plate. The plate used in the experiments was prepared from 25µ sintered stainless-steel particles and had an average porosity of 40 - 45 per cent. Although the porous section is best calibrated under actual tunnel operating conditions, this was not found practical in the present experiments, and instead, the assembled plate and plenum configuration was surveyed under atmospheric external conditions using a constant-temperature hot-wire anemometer and a specially constructed plate-facing pitot tube. The wire used was 0.1 mil diameter platinum-rubidium, mounted between two needles approximately .030 inches apart. The pitot tube used was composed of thin-wall stainless-steel tubing with an outside diameter of about .040 inches.

Very close to the surface, large spatial fluctuations (~50 per cent) in velocity were observed with both the pitot and hot-wire probes. The wave length of the fluctuations was about .04 inches and the mean velocities, calculated for lengths of this order, were found to be within 10 per cent of the overall plate average value, indicating no large-scale non-uniformity. Furthermore, the fluctuations decayed rapidly with distance from the surface, and at a distance of 0.1 inches were within ± 5 per cent of the overall mean value. The decay with distance away from the plate would be expected to be more rapid in the low-density tunnel operating conditions. Finally, and perhaps most important, the overall mean injection velocity at the plate calculated directly from the hot-wire measurements agreed in all cases within ± 5 per cent with the values obtained by taking the measured total mass flow to the plate and dividing by the ambient density and the measured plate surface area. Under tunnel operating conditions, the same agreement should exist between the mass flow per unit area determined by dividing the total (measured) mass flow to the plate by the plate area and that which would be measured directly. Hence, the quoted values of λ_∞ which follow can be considered accurate to within ± 5 per cent (including flowmeter inaccuracies).

Schlieren Results

The first set of tunnel runs were made to determine crudely the nature of the flow field, and only schlieren photographs were taken (with and without side fences). These photographs showed remarkably straight bow shocks and linear growth of the edge of the mixing layers, and hence indicated the possibility that a similar flow field had been established. However, the photographs also indicated that transition regions existed at either end of the porous plate, e. g. see Figure 1. At the upstream end, the transition region required for adjustment of the initial turbulent layer to the injection appeared to occupy about 5 - 7 initial boundary layer thicknesses. At the downstream end, the expansion required by the end of injection appeared to propagate upstream over the porous plate a distance of about two boundary layer thicknesses.

Care was necessary at the higher blowing rates to ensure that separation of the boundary layer did not occur at the downstream edge of the porous plate. Separation was prevented by redesign of the tunnel diffuser and by increasing the pumping capacity of the tunnel.

In addition to this problem of downstream separation, a separation of the initial boundary layer upstream of the porous plate was encountered when the turning angle produced by blowing was greater than about 14°. This result is to be expected from earlier studies of turbulent boundary layer separation.

When all separation phenomena are avoided, the external flow produced by injection resembles that produced by a wall which turns toward the flow through a small angle and then, after a space, returns to its original direction. The transition regions at both turns and the uniform region between are present. This general picture of the flow is confirmed by pitot pressure measurements discussed later.

Static Pressure

Perhaps the most difficult mean flow quantity to determine in this kind of experiment is the static pressure. The use of standard pressure taps in the porous region may give results which are in error due to blowing, and, furthermore, any such taps may cause large non-uniformities in the injection distribution. In an attempt to circumvent this problem, pressure taps were installed on the fences as shown in Figure 2. The question now becomes one of determining the correlation between the values of pressure as measured by the fence taps and the porous-plate static pressure. For no injection, the fence pressure-tap values agreed with the normal static taps ahead of and behind the model within a few per cent.

For the case of injection, the following procedure was followed. First, pitot traces were taken from the wall out to and across the induced shock wave. Figure 3 shows a typical pitot trace taken (with side fences) at an intermediate injection rate. Two points are worth mentioning. The first is that the raw pitot traces were found to be similar when scaled with the thickness as determined from the maximum slope intercept shown in Figure 3: the second is that, unlike normal turbulent boundary-layer pitot profiles, the traces for large injection are quite inflected near the wall (i. e., slowly varying).

Using the measured jump in pitot pressure across the shock wave and knowing free stream conditions, the static pressure and flow deflection angle just behind the shock wave were calculated from the oblique shock equations. The angle was checked with that measured from the schlieren photographs. As seen in Figure 3, the flatness of the pitot trace from the boundary layer edge to the shock for various x-stations and the uniformity of the shock pitot-pressure jump indicate a uniform (constant pressure) flow behind the shock.

Secondly, the fact that the pitot pressure is slowly varying near the wall indicates that, regardless of angle of attack, the flow near the wall has a very small dynamic pressure, and the pitot reading should be close to the static pressure. If this is so, then very near the wall there should be only a negligible effect of pitot orientation. To verify this idea, a pitot tube with an opening facing the plate was constructed and vertical traverses made. Near the wall, good agreement was found between pressure measurements obtained with the modified and standard probes. This results indicates the validity of the above hypothesis.

Finally, all four of these pressure values, i. e., the fence values, the values deduced from the shock jump, the plate-facing pitot value, and the value for the standard pitot at the wall, were compared in the region where similar flow was observed from the raw pitot data. For all injection rates, these data agreed within 8 per cent, and thus show that the fence taps give a valid value of plate static pressure and indicate the absence of any appreciable y-pressure gradient.

In the region near the end of the plate, where the abrupt cessation of injection dominates the flow and causes severe streamline curvature, the readings from the fences were used alone to determine the pressure. As would be expected from the discussion under Schlieren Results, a positive pressure gradient in the y-direction shows the effect on the flow of the rapid expansion near the end of the injection.

Data Reduction

The pitot data were reduced by using the measured static pressure and the Rayleigh pitot formula to calculate the Mach number distribution. No corrections were made for the effect of angle of attack on the pitot data, since at least two other effects must be included in this region to accurately correct the pitot data. The first is the effect of Reynolds number on the reading, because the region of high angle of attack is also the region of low flow velocities and low densities. The second, and probably not as important, effect is that of the wall on this measurement. Hence, the data presented can be expected to be in error (large relative error but small absolute error) near the wall.

The final assumption made concerns the total temperature distribution in the layer. Since both the tunnel and model plenums are at room temperature, it was assumed that the total temperature everywhere in the layer was equal to the ambient value. With these assumptions, then, the velocity profiles were obtained and relevant integral properties were calculated using standard integration techniques and formulae.

III. Experimental Results

Similarity and Two-Dimensionality

Both the pitot tube traces and the schlieren photographs discussed in the previous section suggest that a region of flow over the plate exists where the velocity profiles are self-similar, i. e., scale linearly with the distance along the surface, x. An example of this is shown in Figure 4, where the velocity profiles for an intermediate injection rate are plotted. In Figure 4, the momentum thickness, θ, has been used to normalize the y-coordinate, simply because it is subject to minimum experimental error as compared, for example, with the mixing layer edge. It is seen that in about 5 - 7 initial boundary thicknesses the velocity profiles become independent of x, and that this similarity continues until one reaches the rear region of the plate where the effect of the rapid expansion destroys the similarity.

The question of two-dimensionality of the flow is not as straightforward to decide as is similarity. For example, if the flow is two-dimensional, spanwise pressure measurements taken ahead of and behind the model should be uniform (as indeed they are in these experiments). The converse, however, is not true. Two methods were used to check for the two-dimensionality of the flow. The first was to integrate the continuity equation from the wall to the shock. In this case, one obtains

$$\frac{v_2}{u_2} \equiv \tan\Theta = \frac{d\delta^*_s}{dx} + \lambda_\infty \frac{\rho_\infty u_\infty}{\rho_2 u_2} + \frac{(y_s - \delta^*_s)}{\rho_2 u_2} \frac{d}{dx}(\rho_2 u_2) \qquad (1)$$

where

$$\delta^*_s = \int_0^{y_s} (1 - \frac{\rho u}{\rho_2 u_2}) dy ,$$

$$\lambda_\infty = \frac{\rho_w v_w}{\rho_\infty u_\infty} \qquad (2)$$

Θ = the flow angle behind the shock

y_s = the location of the shock,

and where the subscripts 2 refer to quantities directly behind the shock wave. The quantities contained on each side of equation (1) can be obtained independently from experimental measurements, and since it was found that in the similar region the shock is straight, the last term in equation (1) contributes nothing. Figure 5 presents a check of equation (1). In Figure 5, the angle Θ deduced from the schlieren-measured shock angle and the results obtained by evaluating the right side of equation (1) from the measured velocity profiles is plotted as a function of λ_∞. The good agreement between the values of Θ calculated by the two methods indicates that the flow is very close to two-dimensional.

Figure 5 also shows independently one of the more interesting results of the experiment; Θ, the induced angle of flow deflection due to surface injection. It is seen that for λ_∞ as low as .04, deflection angles greater than 10^o are induced, and these large angles produce significant pressures and side forces. The value of Θ increases very nearly linearly with λ_∞ up to about $\Theta = 12^o$ at λ_∞ = 0.03, and more slowly for larger values of λ_∞. The maximum value obtained is fixed by the upstream separation phenomena described under Schlieren Results.

A second check of two-dimensionality is to consider the integrated x-momentum equation. Assuming a boundary-layer type flow, one obtains, for zero x-pressure gradient, the result

$$\frac{d\theta}{dx} = \lambda_e[1 + C_f/2\lambda_e] . \qquad (3)$$

For the injection rates of this experiment, it can easily be shown that $C_f/\lambda_e << 1$, so that to a first approximation,

$$\frac{d\theta}{dx} \cong \lambda_e \quad \text{or} \quad \theta = \theta_o + \lambda_e x \qquad (4)$$

if the flow is two-dimensional. Figure 6 presents the values of θ obtained from the velocity profiles plotted versus x and the slopes required to agree with equation (4). At the highest injection rate, where the uncertainty in calculating θ is a maximum, the deviation is about 10 per cent, and it is much less at lower injection rates. Hence, both methods indicate that a reasonably two-dimensional flow has been achieved. (Note that without the fences, agreement achieved by either method was much worse.)

Since it has been shown that a similar, two-dimensional flow has been established, the velocity profiles measured in the similar region should be unique, i. e., should be independent of such incidental experimental details as the initial boundary layer thickness, and should only depend on such parameters as Mach number or blowing rate. From equation (1), it is seen that the natural parameter for the blowing rate is $\lambda_e = (\rho_w v_w)/(\rho_e u_e)$ where the subscripts e denote conditions at the edge of the layer ($\rho_e u_e = \rho_2 u_2$ for the uniform external flow caused by a straight shock). Plots of u/u_e versus y/θ are shown in Figure 7. By increasing the value of λ_e, a whole range of profile shapes can be obtained. At the highest injection rate, the velocity profiles are fully inflected and approach the free mixing-layer curve. Note that despite the great change in profile shape, the thickness of the layer, in terms of the momentum thickness, does not change greatly and remains close to $10\,\theta$ for $\lambda_e \geq .004$ (compared with the no injection value at this Mach number $\delta \approx 13\,\theta$).

Compressibility and Turbulent Mixing

Two difficult questions which have not been answered for this type of flow are: first, the question of the effect of density variation across the layer on the mean flow quantities; and second, the process by which the turbulent fluid motion entrains the mass injected at the wall and mixes it with the external flow. Since a direct experimental explanation of the second question in supersonic flow is extremely difficult, it is useful to attempt first to determine the overall effects of compressibility on the mean flow properties. If this can be done, then low-speed experiments, where direct, quantitative measurements of turbulent shearing stress are considerably simplified, can be used to help understand the mixing. At stated previously, the data of McQuaid(2) include moderately high injection rates, and his careful monitoring of pressure by adjusting the tunnel walls ensures a minimum pressure gradient in the flow direction. In addition, because the results of Figure 7 indicate that boundary-layer velocity profiles approach the free mixing-layer values for large injection rates, the mixing layer data of Liepmann and Laufer(4) will also be useful for comparison with the results obtained at the high injection rates.

According to Coles[5], sufficient conditions for transformation of a boundary-layer type flow from a low-speed or incompressible flow (barred quantities) to a compressible flow are:

$$\overline{\psi}/\psi = \sigma(x) \;,\; d\overline{x}/dx = \xi(x) \;,\; \overline{\rho}d\overline{y} = \eta(x)\rho dy . \quad (5)$$

A result of this transformation is

$$\overline{u} = [\sigma(x)/\eta(x)]u \quad (6)$$

which implies that at corresponding points

$$u/u_e = \overline{u}/\overline{u}_e . \quad (7)$$

From (5),

$$\overline{\rho}\overline{y} = \eta(x)\int_0^y \rho dy \quad (8)$$

where we assume $\overline{y}$ $(y = 0) = 0$, i.e., assume wall transforms into wall. The momentum thickness is given by:

$$\theta \equiv \int_0^\infty \frac{\rho u}{\rho_e u_e}\left(1 - \frac{u}{u_e}\right)dy = \frac{1}{\eta(x)}\int_0^\infty \frac{\overline{u}}{\overline{u}_e}\left(1 - \frac{\overline{u}}{\overline{u}_e}\right)\frac{\overline{\rho}}{\rho_e}d\overline{y}$$

or

$$\overline{\rho}\,\overline{\theta} = \eta(x)\rho_e\theta . \quad (9)$$

Combining (8) and (9), one obtains

$$\overline{y}/\overline{\theta} = \int_0^y \frac{\rho}{\rho_e} d(y/\theta) \quad (10)$$

at corresponding stations, which is a general form of the Howarth-Dorodnitsyn transformation.

If the transformation shown in equation (10) is applicable and if the only relevant parameter is the mass flow at the wall normalized by the edge value, λ_e, then the velocity profile $u/u_e\{\overline{y}/\overline{\theta}\}$ obtained at $M_\infty = 2.6$ should agree with the low-speed data obtained for the same value of λ_e (for large injection where $\lambda_e/C_f >> 1$).

Figure 8 shows a comparison of the present data with the subsonic data for the injection rates closely corresponding to McQuaid's experiments. Also shown are the profiles obtained at the largest injection values and the data of Liepmann and Laufer. The good agreement indicates that for large injection rates the normalized velocity profiles do depend only on the properly normalized mass flow rate. Note that at $M_\infty = 2.6$ (compare Figures 7 and 8), the transformation shown in equation (10) gives about a factor of two reduction in scale. Hence, the good agreement between compressible and incompressible data is a sensitive check on the transformation.

The profile obtained at the highest injection value also agrees well with the data of Liepmann and Laufer except near the wall. This discrepancy is to be expected, since the maximum injection rate shown is about 10 - 20 per cent lower than the value obtained for the mixing layer.

The success of the transformation in comparing the velocity profiles suggests that the form parameter $H = \delta^*/\theta$ can be similarly correlated. With the assumption of constant total temperature and the transformation of equation (10), one can show that

$$H_i = \left(\frac{\delta^*}{\theta}\right) = \left[\frac{\gamma-1}{2}M_e^2 + \left(1 + \frac{\gamma-1}{2}M_e^2\right)H_i(\lambda_e)\right] \quad (11)$$

where $H_i = \overline{\delta}^*/\overline{\theta}$ is the value for an incompressible flow. Figure 9 shows the values of H_i determined from equation (11) and the measured values of M_e, δ^*, and θ at $M_\infty = 2.6$, and compares them with the results of McQuaid. The agreement is excellent for the range where overlap exists. Furthermore, at the highest injection rate where the boundary layer is nearly separated, the value of H_i obtained from the experiments is close to the value for separated flows (~ 4). Hence, it appears that H_i can be expressed solely as a function of λ_e for large injection rates regardless of density variation, and that the limiting velocity profile reached at $\lambda_e \approx 0.03$ is the standard mixing-layer profile.

However, an important discrepancy exists between these results and the correlation Alber[6] obtained for compressible mixing layers. In examining the available experimental data on these layers, Alber found that the mass entrained on the low-speed side of these layers was proportional to the square of the density ratio across the layer. In the present experiment, as injection was increased, the velocity profile of the layer approached that of the free mixing layer, but the mass entrained by the supersonic layer, at maximum blowing rate where its velocity profile was similar to that of a mixing layer, was about the same as for the low-speed mixing layer case. In these experiments, the ratio of edge density to that at the wall was about two, and hence Alber's correlation predicts an entrainment rate of about 300 per cent too low.

Clearly, further experiments with a heated or cooled wall, at higher Mach numbers, or with foreign gas injection are necessary to rigorously establish this density independence and the appropriate coordinate transformation. The problem also remains of establishing what would occur to H_i and the velocity profiles if $\lambda_e > 0.03$ could be obtained without the upstream separation occurring. Both these problems are currently being examined at GALCIT.

Flow Angle and Shear Stress Distribution

With similar flow established, it is possible to use the velocity profiles shown in Figure 7 to calculate the flow angles through the layer and the shear stress distribution if one assumes boundary layer flow. The equations in the zero pressure-gradient similar region are:

$$\text{continuity} \quad \frac{\partial}{\partial x}(\rho u) + \frac{\partial}{\partial y}(\rho v) = 0 , \quad (12)$$

$$\text{momentum} \quad \rho u\frac{\partial u}{\partial x} + \rho v\frac{\partial u}{\partial y} = \frac{\partial \tau}{\partial y} . \quad (13)$$

Integrating (12) from $y = 0$ to $y = \tilde{y}$,

$$\frac{v}{u}(\tilde{y}) = \lambda_e\left(\frac{\rho_e u_e}{\rho u}\right) - \left(\frac{\rho_e u_e}{\rho u}\right)\frac{d}{dx}\left\{\int_0^{\tilde{y}}\frac{\rho u}{\rho_e u_e}dy\right\} + \frac{d\tilde{y}}{dx} . \quad (14)$$

For similar flow, $\rho u/\rho_e u_e = f(y/\theta)$ and $d\theta/dx \approx \lambda_e$, so equation (14) gives

$$\frac{v}{u} = \lambda_e\left[\frac{\rho_e u_e}{\rho u} - \left(\frac{\rho_e u_e}{\rho u}\right)\int_0^{\tilde{y}/\theta}\frac{\rho u}{\rho_e u_e}d\left(\frac{y}{\theta}\right) + \frac{\tilde{y}}{\theta}\right] . \quad (15)$$

Similarly, integrating equation (13) and using equation (15), one gets

$$\frac{\tau-\tau_w}{\rho_e u_e^2} = \lambda_e\left\{\frac{u}{u_e}-\frac{u}{u_e}\int_0^{y/\theta}\frac{\rho u}{\rho_e u_e}d\left(\frac{y}{\theta}\right)+\int_0^{y/\theta}\frac{\rho u^2}{\rho_e u_e^2}d\left(\frac{y}{\theta}\right)\right\} \quad (16)$$

where τ_w is the wall shear stress. Figures 10 and 11 show the results of equations (15) and (16) as applied to the data presented in Figure 7. From these equations, one sees that the minimum value of v/u and the maximum value of $(\tau-\tau_w)/(\rho_e u_e^2)$ occur when

$$\int_0^{y/\theta}\frac{\rho u}{\rho_e u_e}d(y/\theta) = 1 \ . \quad (17)$$

The dividing streamline ($\psi = 0$) is defined by the point where

$$\int_0^y \frac{\rho u}{\rho_e u_e}dy = \int_0^x \frac{\rho_w v_w}{\rho_e u_e}dx \ . \quad (18)$$

For constant injection and similar flow with $d\theta/dx = \lambda_e$, equations (17) and (18) are the same if the initial boundary layer is zero thickness. The effect of finite initial boundary-layer thickness is to cause a discrepancy in the measured maximum in shear stress and the dividing streamline location as determined from equation (18). Hence, for a truly similar flow, independent of initial boundary-layer thickness, the maximum value of shear stress, and the minimum flow angles should occur along the dividing streamline. In Figures 10 and 11, the point $\psi = 0$ determined from (18) (a mass balance) is plotted. The close agreement with the maximum of τ and minimum of v/u is still another check on the two-dimensional, similar nature of the experimental flow. It should be emphasized that in using equation (18), x is the actual distance from the beginning of the porous plate and has not been corrected for any virtual origin effects. It might also be noted that factors other than the initial boundary-layer thickness might cause the small bias shown in Figures 10 and 11; for example, the assumption of constant total temperature or the effect of pitot probe angle of attack might be responsible.

Figure 10 also indicates the region where large errors in the pitot tube readings are important due to angle of attack effects. The most important result shown in Figure 11 is that, although the shear stress at the wall is expected to be quite small, the maximum shear stress in the layer is several times the maximum value in the boundary layer with no injection, and this result emphasizes the importance of turbulent mixing in this problem. For example, for the approaching boundary layer at the Reynolds number and Mach number of these tests ($Re\theta \sim 2000$, $M_e = 2.6$),

$$C_{fo} = \left.\frac{2\tau_w}{\rho_e u_e^2}\right)_{\lambda_e = 0} \approx .0025 \ .$$

At the highest injection rate shown in Figure 11,

$$\left.\frac{\tau_{max}}{\rho_e u_e^2}\right)_{\lambda_e = .029} \approx .01 \ ,$$

and this value is about four times larger than C_{fo}. If one assumes Newtonian shearing stress, then at the wall one obtains (from Figure 7):

$$[\partial(u/u_c)/\partial(y/\theta)]_{\lambda_e \cong .029} \approx .05$$

So,

$$\left.\frac{\tau_w}{\rho_e u_e^2}\right)_{\lambda_e = .029} = \frac{1}{Re\theta}\left(\frac{\mu_w}{\mu_e}\right)\frac{\partial(u/u_e)}{\partial(y/\theta)} \approx 10^{-5}$$

for the value of θ given in Figure 7 and Re/inch $\approx 2.2 \times 10^5$. Hence, for these high injection rates, the wall stress is of no importance. The important boundary condition at the wall is the entrainment which is prescribed by the injection rate.

Induced Side Forces

Another result which can be obtained from the data is the induced side forces caused by the interaction of the injectant with the external stream. Assuming that $C_f/\lambda_e \ll 1$ and that $H_i = \overline{\delta^*}/\overline{\theta}$ can be expressed only as a function of λ_e (regardless of density ratio across the layer) and using a Crocco integral relation for the total enthalpy in the layer, Lees(7) has combined the integral form of the boundary-layer continuity and momentum equations to obtain the following expression for the induced angle:

$$\tan\Theta = \lambda_e\left(1+\frac{\gamma-1}{2}M_e^2\right)\left[1+\frac{T_w}{T_{t\infty}}H_i\{\lambda_e\}\right]. \quad (19)$$

By an iterative process, it is possible to obtain $\Theta\{\lambda_e, M_e\}$ or $\Theta\{\lambda_\infty, M_\infty\}$ from the above equation and Figure 9.

Calculations of the total side force produced by injection were made without taking account of up- and downstream end effects, and consequently the total force for a plate of length L and unit width was calculated from $F = (P_e\{\Theta\} - P_\infty)L$. Values of F normalized by the thrust of a sonic jet of the same mass flow rate flowing into a vacuum, F_{sv}, were calculated for $2.6 \le M_\infty \le 8$; $0 \le \Theta \le 14^\circ$; $\gamma = 1.4$, and $0.33 \le T_w/T_{t\infty} \le 1.5$.

As would be expected from the excellent agreement between calculated and measured values of $\Theta\{\lambda_\infty\}$, shown in Figure 5, calculated and experimental values of F/F_{sv} for the $M_\infty = 2.6$ case agree well. The thrust ratio increased from 2.9 for very small values of λ_e to 3.5 at the maximum blowing rate of $0.03 = \lambda_e$. In addition, calculated values of F/F_{sv} were within ± 10 per cent of 3.2 for the whole range of parameters examined in the calculations. This value is slightly larger than similarly normalized side forces obtained experimentally for concentrated injection of gases from narrow slots and into supersonic streams(8).

Effect of the Finite Plate Length

Since the effect of large injection is to cause inflection of the mean velocity profiles and to move the sonic line away from the wall, the fact that the porous plate is finite in length could be felt upstream. The termination of injection causes an abrupt expansion of the flow with noticeable pressure variations normal to the wall and large pressure gradients in the streamwise direction. This effect is also readily observed in the velocity profiles.

For all injection rates examined, the effect of the rapid expansion propagates about two final layer thicknesses upstream. Since the induced angles depend only on λ_e and M_e, it seems reasonable to suppose that, in any experiment which attempts to investigate higher injection rates than the present values, the "few" thicknesses which are influenced by the end of the porous region will essentially cover the entire porous plate. For example, if the induced angle is 20°, and if the corner effect propagates upstream two layer thicknesses, then it is easily seen that regardless of the plate length, about 75 per cent of the plate will be dominated by the effect of the termination of injection.

Hence, any theoretical analysis of the flow field produced by injection rates much larger than the maximum used here must include this downstream interaction region. In this case, the flow will not be similar over most of the injection region.

IV. Conclusions

(1) A self-similar, two-dimensional flow field with linear growth has been established experimentally and its mean flow properties have been investigated.

(2) The results obtained at $M_\infty = 2.6$ can be brought into agreement with the available incompressible data on boundary layers with moderately large injection by using a Howarth-Dorodnitsyn type transformation.

(3) At the highest injection rate, the mean velocity profiles approach the free mixing-layer results. However, the amount of mass entrained at this point seems independent of density differences across the layer.

(4) Forces obtained with distributed injection are comparable to those obtained with injection through a slot for a given total mass flow rate.

(5) At induced flow angles greater than about 14°, upstream separation of the boundary layer is observed. For any finite, porous plate length, the effect of the discontinuity in injection at the end of the region is felt increasingly farther upstream and is expected to dominate the entire flow field for induced flow angles greater than $\approx 20°$.

References

1. Hartunian, R. A. and Spencer, D. J., "Experimental Results for Massive Blowing Studies," AIAA Journal, Vol. 5, No. 8 (August 1967), pp. 1397-1401.

2. McQuaid, J., "Incompressible Turbulent Boundary Layers with Distributed Injection," Ph. D. Thesis, Engineering Department, Cambridge University (September 1966).

3. Mugalev, V. P., "The Experimental Investigation of the Subsonic Turbulent Boundary Layer on a Plate with Injection," Izvestiia Vysshikh Uchebnykh Zavedonii; Ayiationnaya Tekhnika, No. 3 (1959), pp. 72-79 (translated by J. B. Gazley), Rand Corp. Report T-142 (Dec. 8, 1960).

4. Liepmann, H. W. and Laufer, J., "Investigation of Free Turbulent Mixing," NACA TN 1257 (August 1947).

5. Coles, D. F., "The Turbulent Boundary Layer in a Compressible Fluid," Rand Corp. Report R-403-PR (September 1962).

6. Alber, I. E., "Integral Theory for Turbulent Base Flows at Subsonic and Supersonic Speeds," Ph. D. Thesis, Aeronautics Department, California Institute of Technology (May 1967).

7. Lees, L., "Surface Mass Injection at Supersonic and Hypersonic Speeds as a Problem in Turbulent Mixing: Part I. Two-Dimensional Flow," TRW Report 06388-6021-R000 (August 1967).

8. Spaid, F. and Zukoski, E. E., "A Study of the Interaction of Gaseous Jets from Transverse Slots with Supersonic External Flow," accepted for publication in AIAA Journal.

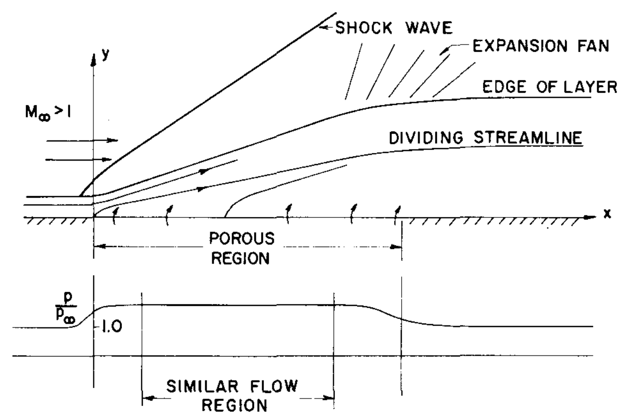

Fig. 1. Schematic of Flow Field.

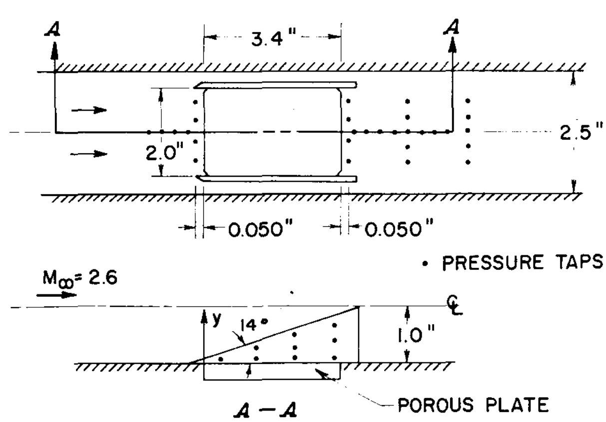

Fig. 2. Schematic of Model in Tunnel.

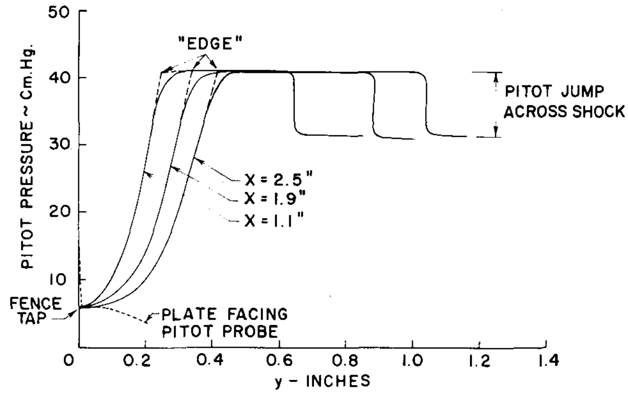

Fig. 3. Pitot Trace Showing Check for Fence Pressure Tap Reading (λ_∞ = .015).

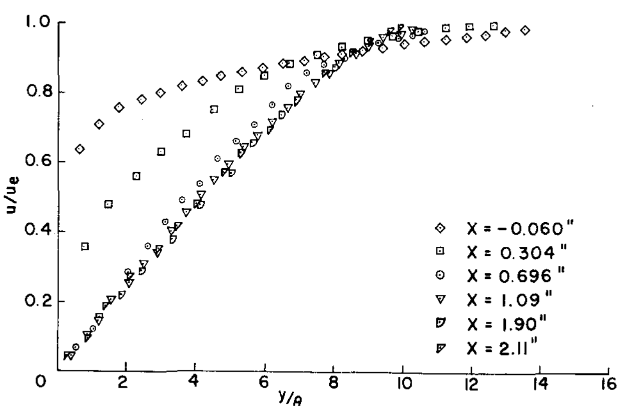

Fig. 4. Approach to Similar Flow (λ_∞ = .015, λ_e = .0126).

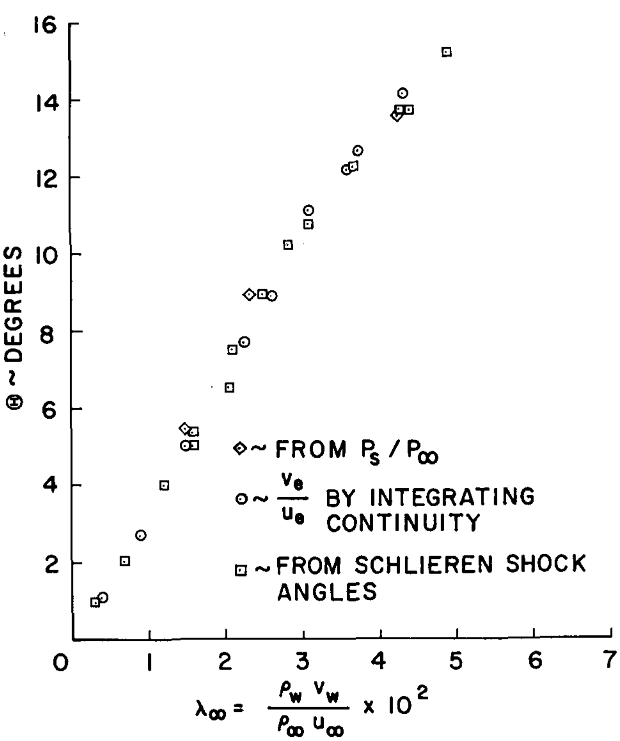

Fig. 5. Induced Flow Angle.

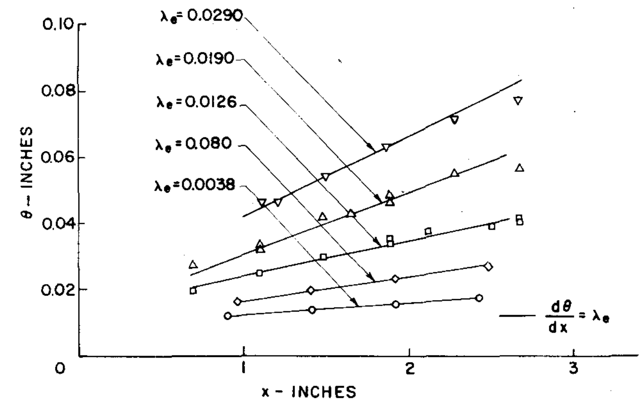

Fig. 6. Momentum Thickness.

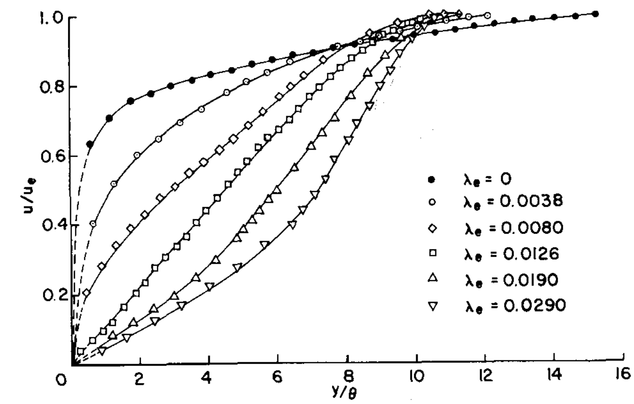

Fig. 7. Effect of Injection on Velocity Profiles.

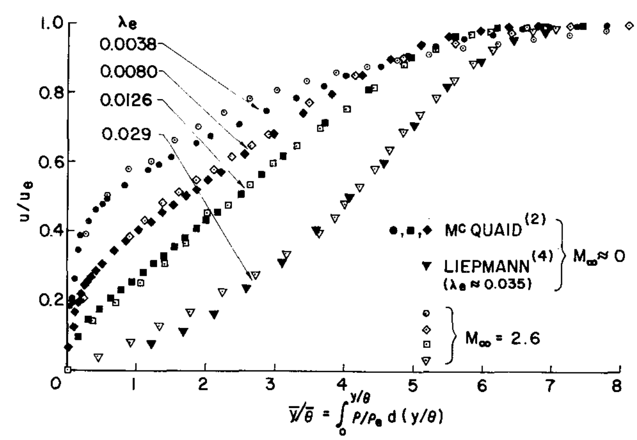

Fig. 8. Comparison with Low Speed Data.

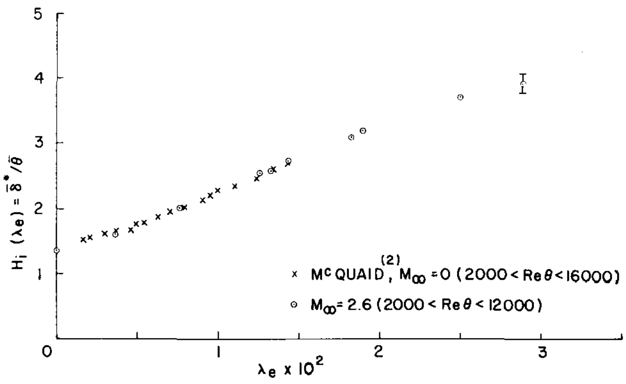

Fig. 9. Form Parameter Comparison.

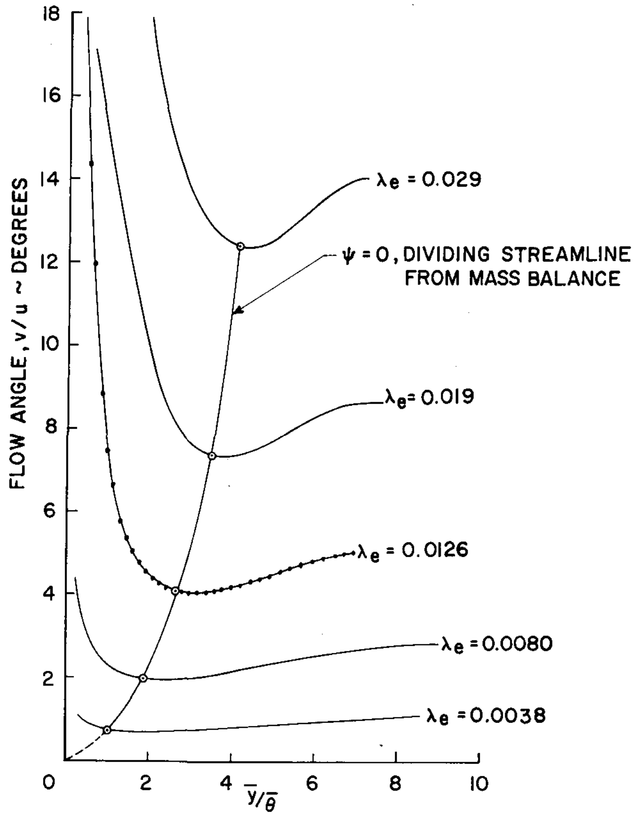

Fig. 10. Flow Angles.

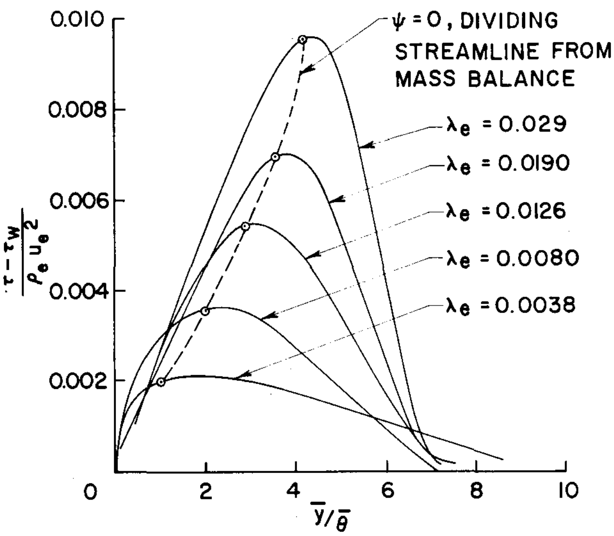

Fig. 11. Boundary Layer Shear Stress.